

Superconducting contacts to a monolayer semiconductor

M. Ramezani,^{†,‡} I. Correa Sampaio,[†] K. Watanabe,[¶] T. Taniguchi,[§] C. Schönenberger,^{†,‡} and A. Baumgartner^{*,†,‡}

[†]*Department of Physics, University of Basel, CH-4056, Basel, Switzerland*

[‡]*Swiss Nanoscience Institute, University of Basel, CH-4056, Basel, Switzerland*

[¶]*Research Center for Functional Materials, National Institute for Material Science, 1-1 Namiki, Tsukuba, 305-0044, Japan*

[§]*International Center for Materials Nanoarchitectonics, National Institute for Materials Science, 1-1 Namiki, Tsukuba 305-0044, Japan*

E-mail: andreas.baumgartner@unibas.ch

Abstract

We demonstrate superconducting vertical interconnect access (VIA) contacts to a monolayer of molybdenum disulfide (MoS_2), a layered semiconductor with highly relevant electronic and optical properties. As a contact material we use MoRe, a superconductor with a high critical magnetic field and high critical temperature. The electron transport is mostly dominated by a single superconductor/normal conductor junction with a clear superconductor gap. In addition, we find MoS_2 regions that are strongly coupled to the superconductor, resulting in resonant Andreev tunneling and junction dependent gap characteristics, suggesting a superconducting proximity effect. Magnetoresistance measurements show that the bandstructure and the high intrinsic carrier mobility remain intact in the bulk of the MoS_2 . This type of VIA contact is applicable to a large variety of layered materials and superconducting

contacts, opening up a path to monolayer semiconductors as a platform for superconducting hybrid devices.

keywords: *TMDC, van der Waals heterostructure, MoS₂, monolayer semiconductor, superconducting contacts, superconducting proximity effect*

Semiconductors combined with superconducting metals have become a most fruitful field for applications and fundamental research, from gate tunable superconducting qubits,¹ thermoelectrics,^{2,3} to prospective Majorana bound states,^{4,5} or sources of entangled electron pairs.⁶⁻⁸ These experiments were mainly developed based on one-dimensional (1D) nanowires. To obtain more flexible platforms and scalable architectures, recent efforts focused on two-dimensional (2D) semiconductors.⁹⁻¹³ However, the number of materials suitable for superconducting hybrids is rather limited. Potentially ideal and ultimately thin semiconductors with a large variety of properties can be found among transition metal dichalcogenides (TMDCs) grown in stacked atomically thin layers. TMDCs often exhibit a broad variety of interesting optical and electronic properties,¹⁴⁻¹⁶ for example the valley degree of freedom, potentially useful as qubits,^{17,18} strong electron-electron^{19,20} and spin-orbit interactions,²⁰ or crystals with topologically non-trivial bandstructures.^{21,22} One promising material is the semiconductor MoS₂, with a relatively high mobility and large mean free path, allowing for gate-defined nanostructures,²³⁻²⁵ which would make MoS₂ an ideal platform to combine with superconducting elements.

MoS₂ was used as tunnel barrier between superconductors in vertical heterostructures^{26,27} and showed signs of intrinsic superconductivity²⁸ and of a ferromagnetic phase at low electron densities.²⁹ However, to exploit the intrinsic properties of MoS₂ and to fabricate in-situ gate tunable superconducting hybrid structures, direct superconducting contacts in lateral devices are required. Such contacts are difficult to fabricate due to the formation of Schottky barriers,^{21,30,31} material degradation³² and fabrication residues when using standard fabrication methods.^{24,33,34} Less conventional edge contacts were also found problematic recently.³⁵

Here, we report vertical access interconnect (VIA) contacts³⁶ to monolayer MoS₂ with the superconductor MoRe as contact material. We demonstrate a clear superconducting gap in the transport characteristics, including the magnetic field and temperature dependence, and features suggesting stronger superconductor-semiconductor couplings, forming the basis for superconducting proximity effects and bound states. In addition, we show that this fabrication method retains the intrinsic MoS₂ bulk properties, including a large electron mobility and sequentially occupied

spin-orbit split bands.²³

Figure 1(a) shows an optical microscopy image of the presented device, and a schematic of a single VIA contact. The MoS₂ is fully encapsulated by exfoliated hexagonal boron nitride (hBN), ensuring minimal contamination of the bulk materials, while the following assembly process allows the fabrication of pristine material interfaces and contacts:

1) vertical access: using electron beam lithography (EBL), VIA areas with a radius of 200 nm are defined on the designated top hBN flake (~ 40 nm thickness) on a Si/SiO₂ wafer, and etched completely open by reactive ion etching with a 20:5:5 sccm SF₆:O₂:Ar mixture at 25 mTorr chamber pressure and 50 W RF power.

2) VIA metalization: in a second EBL step, a slightly larger area with the VIA in the center is defined for mechanical anchoring to the top hBN. We then deposit the type II superconductor MoRe (bulk critical temperature $T_c \approx 6 - 10$ K, (second) critical magnetic field $B_c \approx 8 - 9$ T^{37,38}) using sputter techniques. As the optimal film thickness we find 10 nm plus the top hBN thickness.

3) Stacking of layers: the wafer with the VIA structure is transferred to an inert gas (nitrogen) glove box, where the top hBN layer with the metalized VIAs is picked up from the substrate using a polycarbonate (PC) stamp and an hBN helper layer, and then used to pick up consecutively a monolayer MoS₂ flake, a bottom hBN flake (~ 25 nm thickness), and a multilayer graphene (MLG) flake serving as backgate.

4) Finish: the stack is then deposited onto a Si/SiO₂ wafer, where macroscopic Ti/Au (10/50 nm) leads to the VIAs are fabricated using EBL. The sample is then annealed at 350°C for 30 min, in a vacuum chamber with a constant flow of forming gas.

Using gold as VIA material, this fabrication process yields $> 80\%$ of the contacts with two-terminal resistance-area products smaller than $200 \text{ k}\Omega\mu\text{m}^2$ at $T = 1.7$ K at a backgate voltage of $V_{BG} = 10$ V. This yield is reduced to roughly 50% when using MoRe, possibly due to a material loss during the pick-up procedure. In the presented device, only half of the contacts show resis-

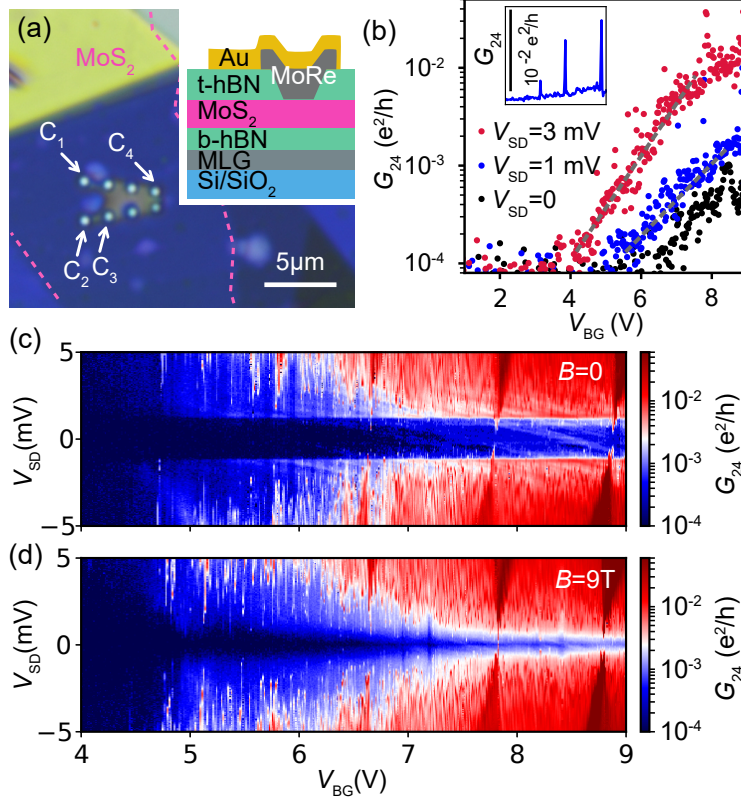


Figure 1: (a) Optical microscopy image of the MoS₂ heterostructure, with MoRe VIA contacts pointed out by white arrows. Inset: schematic of a VIA contact, with t-hBN and b-hBN denoting the top and bottom hBN layers, respectively. (b) Differential conductance G_{24} as a function of V_{BG} for a series of V_{SD} on a logarithmic scale, and as an inset for $V_{SD} = 1$ mV on a linear scale. (c) G_{24} vs. V_{BG} and V_{SD} at $B = 0$ and (d) at $B = 9$ T.

tances lower than $200 \text{ k}\Omega \mu\text{m}^2$, which we use for the experiments and are labeled from C_1 to C_4 in Fig. 1(a). The two terminal differential conductances $G_{jk} = dI_j/dV_k$ we obtain by measuring the current variation in the grounded contact C_j while applying a modulated bias voltage V_{SD} to contact C_k using standard lock-in techniques. The experiments were performed in a dilution refrigerator at ~ 60 mK, while for higher temperatures, we used a variable temperature insert (VTI) with a base temperature of ~ 1.7 K. In addition, we apply an external magnetic field B perpendicular to the substrate.

In Fig. 1(b), the differential conductance G_{24} is plotted as a function of the backgate voltage V_{BG} for several bias voltages V_{SD} . Increasing V_{BG} results in an exponential increase in G_{24} , starting from a pinch-off voltage of $V_{BG} \approx 6$ V for $V_{SD} = 0$. This value is offset towards smaller values for

larger bias voltages, a first indication for an energy gap. However, as seen in the inset of Fig. 1(b), in this regime we find very sharp peaks in G , consistent with Coulomb blockade (CB) effects. We note that an increase in V_{BG} not only changes the charge carrier density in the MoS_2 , but also the Schottky barrier at the metal-semiconductor interface and disorder induced charge islands. To demonstrate a superconducting energy gap and to distinguish it from other effects like CB, we plot in Fig. 1(c) the conductance G_{24} vs. V_{SD} over a large range of V_{BG} at $B = 0$, while Fig. 1(d) shows the same experiment at $B = 9\text{T}$. At $B = 0$, independent of the gate voltage, one clearly finds a strongly suppressed conductance for roughly $|V_{\text{SD}}| < 1.2\text{mV}$, a gap size consistent with literature values for the superconducting energy gap of MoRe .³⁹ The conductance is suppressed by a factor ~ 8 between the large and the zero bias values at $V_{\text{BG}} \approx 6\text{V}$, and by a factor of ~ 15 near $V_{\text{BG}} = 8\text{V}$. We note that such a sharp gap is only observable if a tunnel barrier is formed between the semiconducting MoS_2 and the superconducting region, at least at one contact. The discrete features inside the gap are probably not Andreev bound states,^{40,41} but rather originate from gate-modulated conductance features in the bulk MoS_2 . At $|V_{\text{SD}}| > 1.2\text{mV}$, we find a strong modulation of G , which we interpret as several Coulomb blocked regions. These resonances suggest that there is significant disorder near some of these contacts, so that we can think of this device as an MoS_2 region, incoherently coupled to the contacts by two normal-superconductor (N/S) junctions. The reason for one junction, namely the less transparent one, dominating the transport characteristics is that the junction with the higher transmission has a reduced resistance in the energy gap due to Andreev reflection, in which two electrons are transferred to S to form a Cooper pair. At $B = 9\text{T}$, the superconducting gap is reduced, as discussed below in detail, but we now find that the gap becomes gate dependent. While in short semiconducting nanowires a gate tunable proximity effect was reported,^{42,43} we tentatively attribute our finding to a gate independent superconducting energy gap convoluted with a gate tunable MoS_2 conductance.

We investigate the gap in the transport characteristics and the field dependence in more detail in Fig. 2 for the same contact pair. Figures 2(a)-(c) show higher resolution conductance maps for a smaller V_{BG} interval, for the magnetic fields $B = 0$, $B = 5\text{T}$ and $B = 9\text{T}$, respectively. The figures

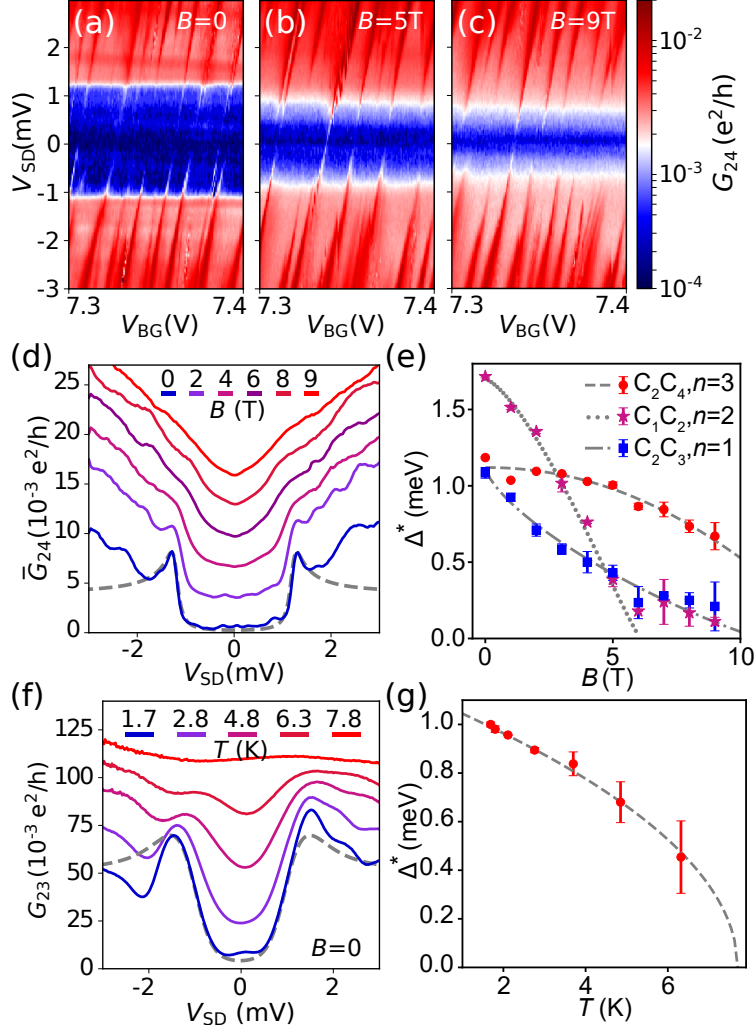


Figure 2: (a) Differential conductance G_{24} as a function of the bias V_{SD} and the backgate voltage V_{BG} at $B = 0$, (b) $B = 5$ T, and (c) $B = 9$ T. (d) G_{24} averaged over a V_{BG} interval of 0.5 V plotted vs. V_{SD} for the indicated magnetic fields, with the curves offset for clarity. (e) Superconducting energy gap Δ^* as a function of B for different contact pairs. Δ^* is extracted from the inflection points in the curves of Fig. 2(d) [red disks], from Fig. 3 [purple stars] and from an additional data set discussed in the supplemental data, Fig. S1 [blue rectangles]. (f) G_{23} vs. V_{SD} recorded at the indicated temperatures T . (g) Δ^* vs. T extracted from the data in (f). All theoretical curves (dashed and dotted lines) are discussed in the text.

show a very clear gap in the conductance map, which is systematically reduced with increasing magnetic field, independently of the sharp resonances. The positions of the latter are unaffected by the gap, so that we can attribute them to resonances in the MoS_2 , for example due to CB. To extract the energy gap, we plot G_{24} in Fig. 2(d), averaged over a gate voltage interval of 0.5 V for each V_{SD} value, for a series of perpendicular magnetic fields. These curves show how the energy gap closes

with increasing B . The curve at $B = 0$ can be fitted well using the model by Blonder, Tinkham and Klapwijk (BTK),⁴⁴ including an additional broadening parameter,⁴⁵ as shown in Fig. 2(d) by a gray dashed line. The fit parameters are consistent with a weakly transmitting barrier in a single N/S junction. At larger fields, the extracted parameters become ambiguous due to a strong broadening of the curves. As a measure for the superconducting energy gap Δ^* , we therefore plot in Fig. 2(e) the average of the low-bias inflection points of each curve (red dots). For $B = 0$, we find $\Delta_0^* \approx 1.2$ meV, in good agreement with bulk MoRe^{26,39} and one S/N junction dominating the transport. The field dependence of Δ^* is well described by standard theory of superconductivity for pair breaking impurities in a metal with a mean free path shorter than the superconducting coherence lengths. For the corresponding self-consistency equations we use $\Delta^*(\alpha) = \hat{\Delta}(\alpha)[1 - (\alpha/\hat{\Delta}(\alpha))^{2/3}]^{3/2}$, with $\Delta^*(\alpha)$ the energy gap in the excitation spectrum and $\hat{\Delta}$ the order parameter determined numerically from $\ln(\hat{\Delta}(\alpha)/\Delta_0) = -\pi\alpha/4\hat{\Delta}(\alpha)$ for a given pair breaking parameter α .^{46,47} The latter we interpolate as $\alpha = 0.5\Delta_0^*(B/B_c)^n$, with n a characteristic exponent. As shown in Fig. 2(e), the best fit we obtain for $n = 3$, $\Delta_0^* = 1.12$ meV and the (upper) critical field $B_c = 14.5$ T. The latter value is clearly larger than reported for bulk MoRe. Seemingly similar data plotted as purple stars and blue rectangles we discuss below.

As expected for a superconducting energy gap, Δ^* is also reduced with increasing temperature T . In Fig. 2(f) we plot G_{23} as a function of V_{SD} at $V_{BG} = 9$ V for a series of temperatures at $B = 0$ in a different cooldown. For the lowest values of T , we can reproduce the data using very similar BTK and Dynes parameters as above, only adjusting the normal state resistance and the temperature to $T = 1.7$ K. However, at higher temperatures, the fits become ambiguous, due to a broadening and possibly a temperature dependence of the Schottky barrier.³⁰ Again, we plot the inflection points of the curves as an estimate for Δ^* , as shown in Fig. 2(g). To determine the critical temperature, we fit the expression $\Delta^* = \Delta_0^*\sqrt{1 - T/T_c}$ and find $T_c = 7.7$ K and $\Delta^* = 1.2$ meV, consistent with literature values for bulk MoRe.^{38,39}

Up to this point, our experiments demonstrate superconducting contacts, but with a weak electronic coupling between the MoS₂ and the reservoirs, at least for one contact junction. However,

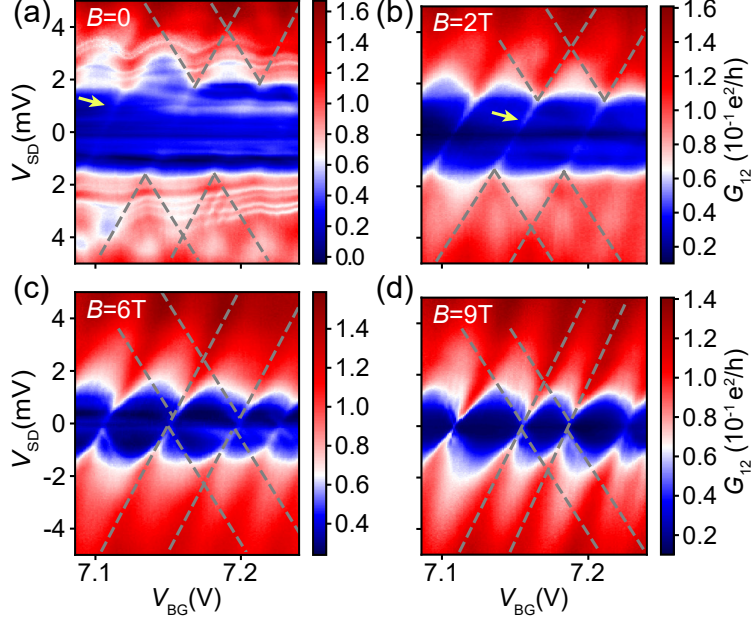


Figure 3: G_{12} plotted as a function of V_{BG} and V_{SD} at (a) $B = 0$, (b) $B = 2$ T, (c) $B = 6$ T and (d) $B = 9$ T, recorded at $T = 60$ mK. The dashed lines trace the CB diamonds, shifted vertically and horizontally between the subfigures, while the yellow arrows point out lines of resonant Andreev tunneling.

we also find evidence for a stronger coupling of MoS₂ regions to the superconductors, relevant for devices relying on the superconducting proximity effect. As an example, we show bias spectroscopy measurements with CB features between contacts C_1 and C_2 in Fig. 3, for a series of magnetic fields B . Similarly as in Fig. 2, we find a transport gap, reduced by larger B values. Here, the low-bias ends of the CB diamonds are shifted in energy and in gate voltage, as indicated by the gray dashed lines, consistent with a MoS₂ quantum dot (QD) directly coupled to one superconducting contact (i.e. forming an S-QD-N junction).⁴⁸ These tips of the CB diamonds are connected across the gap by a single faint resonance, pointed out by yellow arrows, best seen in Fig. 3(b) at $B = 2$ T. We attribute these lines to resonant Andreev tunneling,⁴⁸ in which the electrons of a Cooper pair pass through the QD in a higher order tunneling process. This process is suppressed much stronger by a tunnel barrier than single particle tunneling,⁴⁹ which suggests that the QD is strongly coupled to the superconductor. At large B fields, a quasi-particle background in the superconducting density of states results in single particle CB diamonds.⁴² With a QD charging energy of ~ 2 meV and using $E_c = \frac{e^2}{8\epsilon\epsilon_0 r}$ for a disc shaped QD encapsulated in hBN, we estimate

the radius of the confined QD region as $r \approx 300$ nm.

The shift of the CB diamonds in V_{SD} gives a measure for Δ^* ,⁴⁸ which we read out at the bias at which $\sim 50\%$ of the large bias conductance is reached at the tip of the CB diamond. The extracted values are plotted as purple stars in Fig. 2(e). Surprisingly, we find a significantly larger zero field gap, $\Delta_0^* \approx 1.7$ meV, and a rather different functional dependence on B than for the curves analyzed in Fig. 2 (red dots). The latter is demonstrated by the dotted line obtained for the exponent $n = 2$, and $B_c = 6.4$ T. In addition, Fig. 2(e) shows a third Δ^* curve extracted from CB diamond shifts in experiments on another contact pair shown in the supplemental data, Fig. S1. For this curve, we obtain $n = 1$, while $\Delta^* \approx 1.12$ meV and $B_c \approx 12$ T correspond well to the previously obtained values.

While a larger gap in the transport experiments can be simply attributed to a significant fraction of the bias developing across another part of the device, for example across the second N/S junction, the different functional dependence is more difficult to explain. Since nominally the geometry and MoRe film thickness are identical for all contacts, we tentatively attribute this finding to a superconducting proximity region forming in the MoS₂ near a strongly coupled contact, yielding an induced superconducting energy gap Δ^* ,⁴² and a different B -field dependence of the pair breaking compared to the bulk superconductor.

Additional indications for a stronger coupling to S are the almost gate voltage independent features at $B = 0$, reminiscent of two NS junctions and multiple Andreev reflection processes in between, with a much stronger suppression with increasing B than for the observed gap. In the supplemental data, Fig. S2(a), we also show data at higher gate voltages, exhibiting a conductance minimum instead of a maximum at the bias that corresponds to the energy gap, developing into negative differential conductance at the lowest field values. These findings are qualitatively consistent with calculations for an S/I/N/S junction with resonances in the N region.⁵⁰

The above data show that our fabrication scheme results in superconducting contacts to monolayer MoS₂, possibly with a reasonably strong coupling to the superconductors for some of the contacts. To demonstrate that the intrinsic properties of MoS₂ are intact in the bulk crystal, we in-

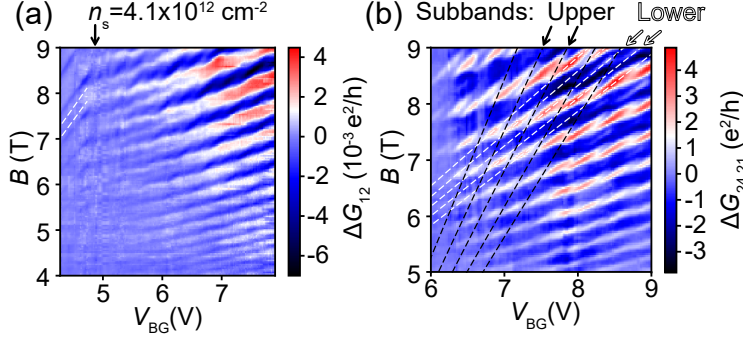


Figure 4: (a) Two-terminal dc conductance $G_{12} = I_1/V_{SD}$ with $V_{SD} = 8$ mV applied to contact C_2 , plotted as a function of the magnetic field B and the backgate voltage V_{BG} at $T \approx 60$ mK. n_s points out the gate voltage corresponding to the electron density at which the higher spin-orbit subbands start to be populated. (b) Three-terminal dc conductance $G_{24,21} = I_2/V_{12}$, with an external bias $V_{SD} = 10$ mV applied to C_4 , while the current I_2 is measured at C_2 and the voltage difference V_{12} between C_1 and C_2 . In both maps, a third order polynomial was subtracted at each gate voltage to remove a smooth background.

investigate quantum transport in large magnetic fields and at bias voltages large enough to render the superconducting energy gap irrelevant. In Fig. 4(a) we plot the dc conductance $G_{12} = I_1/V_{SD}$ as a function of V_{BG} and B , at $V_{SD} = 8$ mV and $T = 60$ mK, from which we have subtracted a third order polynomial background for each gate voltage to eliminate effects from the classical Hall effect and CB effects.

Figure 4(a) shows well developed Shubnikov de Haas (SdH) oscillations, suggesting a high MoS₂ quality, with an onset at $B_{on} < 4$ T. In the Drude model, this onset is interpreted as the charge carriers closing a cyclotron orbit before being scattered, which happens roughly at $\omega_c \tau > 1$, with $\omega_c = eB/m^*$ the cyclotron frequency, m^* the effective electron mass, and τ the scattering time. This yields a lower bound for the carrier mobility of $\mu = e\tau/m^* \approx 2500$ cm²/(Vs), similar to $\mu \approx 5000$ cm²/(Vs) we obtain with Au VIA contacts, identical to the best literature values.²⁴ The discrepancy in mobility between the MoRe and the Au VIA contacts we attribute to heating effects due to the much larger bias we apply to the MoRe contacts to avoid effects of the superconducting energy gap.

The quality of the MoS₂ can also be seen in the fact that the the four lowest spin-orbit subbands, corresponding to the valley and the spin degree of freedom, are not mixed by disorder. We find that

the slope of the SdH resonances changes by roughly a factor of two at $V_{\text{BG}}^* = 4.8 \text{ V}$, corresponding to an electron density of $n_s \approx 4.1 \times 10^{12} \text{ cm}^{-2}$, at which the two upper spin-orbit subbands become populated. Using $m^* = 0.6$, we obtain a subband spacing of $\sim 15 \text{ meV}$, as reported previously.²³ These features prevail also at $T \approx 1.7 \text{ K}$, as shown in the supplemental data, Fig. S2(b).

The two-terminal magneto-conductance measurements suffer from large background resistances due to Shottky barriers, which we can partially circumnavigate by performing a three terminal experiment. In Fig. 4(b) we plot the dc conductance $G_{24,21}$, as explained in the figure caption. This technique removes the contact resistance at C4, so that the conductance resonances due to the Landau levels can be measured more clearly. The results in Fig. 4(b) show similar patterns as in better suited Hall bar experiments,²³ exhibiting clear superposition patterns of the spin and valley split subbands, indicated by dashed lines. We note that due to the less ideal contact geometry of our devices, we cannot go to lower electron densities in these experiments, because the current density passing near the remote contacts is very low.

In conclusion, we established superconducting contacts to a monolayer of the TMDC semiconductor MoS₂ using vertical interconnect access (VIA) contacts, and characterized the superconducting energy gap in different transport regimes. The fact that in most experiments one N/S junction dominates the transport characteristics, and signatures of resonant Andreev tunneling and a superconducting proximity effect, suggest that also contacts with a stronger transmission between the superconductor and the semiconductor are possible, thus opening a path towards semiconductor-superconductor hybrid devices at the limit of miniaturization, with a group of materials - the TMDCs - that offers a very large variety of material properties and physical phenomena.

Associated content

The supplemental data mentioned in the text as Figs. S1 and S2 are available free of charge on the ACS Publications website at DOI:

Acknowledgments

This work was supported financially by the Swiss National Science Foundation project "Two-dimensional semiconductors for superconductor hybrid nanostructures" granted to AB, the Swiss Nanoscience Institute (SNI) project P1701, and the ERC project Top-Supra (787414). K.W. and T.T. acknowledge support from the Elemental Strategy Initiative conducted by the MEXT, Japan, Grant Number JPMXP0112101001, JSPS KAKENHI Grant Numbers JP20H00354 and the CREST (JPMJCR15F3), JST.

References

- (1) Larsen, T. W.; Petersson, K. D.; Kuemmeth, F.; Jespersen, T. S.; Krogstrup, P.; Nygård, J.; Marcus, C. M. Semiconductor-nanowire-based superconducting qubit. *Phys. Rev. Lett.* **2015**, *115*, 127001.
- (2) Leivo, M.; Pekola, J.; Averin, D. Efficient Peltier refrigeration by a pair of normal metal/insulator/superconductor junctions. *Appl. Phys. Lett.* **1996**, *68*, 1996.
- (3) Roddaro, S.; Pescaglioni, A.; Ercolani, D.; Sorba, L.; Giazotto, F.; Beltram, F. Hot-electron effects in InAs nanowire Josephson junctions. *Nano Research* **2011**, *4*, 259.
- (4) Mourik, V.; Zuo, K.; Frolov, S. M.; Plissard, S.; Bakkers, E. P.; Kouwenhoven, L. P. Signatures of Majorana fermions in hybrid superconductor-semiconductor nanowire devices. *Science* **2012**, *336*, 1003.
- (5) Deng, M.; Vaitiekėnas, S.; Hansen, E. B.; Danon, J.; Leijnse, M.; Flensberg, K.; Nygård, J.; Krogstrup, P.; Marcus, C. M. Majorana bound state in a coupled quantum-dot hybrid-nanowire system. *Science* **2016**, *354*, 1557.

- (6) Hofstetter, L.; Csonka, S.; Nygård, J.; Schönenberger, C. Cooper pair splitter realized in a two-quantum-dot Y-junction. *Nature* **2009**, *461*, 960.
- (7) Hofstetter, L.; Csonka, S.; Baumgartner, A.; Fülöp, G.; d'Hollosy, S.; Nygård, J.; Schönenberger, C. Finite-bias Cooper pair splitting. *Phys. Rev. Lett.* **2011**, *107*, 136801.
- (8) Fülöp, G.; d'Hollosy, S.; Baumgartner, A.; Makk, P.; Guzenko, V.; Madsen, M.; Nygård, J.; Schönenberger, C.; Csonka, S. Local electrical tuning of the nonlocal signals in a Cooper pair splitter. *Phys. Rev. B* **2014**, *90*, 235412.
- (9) Wan, Z.; Kazakov, A.; Manfra, M. J.; Pfeiffer, L. N.; West, K. W.; Rokhinson, L. P. Induced superconductivity in high-mobility two-dimensional electron gas in gallium arsenide heterostructures. *Nat. Commun.* **2015**, *6*, 7426.
- (10) Casparis, L.; Connolly, M. R.; Kjaergaard, M.; Pearson, N. J.; Kringhøj, A.; Larsen, T. W.; Kuemmeth, F.; Wang, T.; Thomas, C.; Gronin, S., et al. Superconducting gatemon qubit based on a proximitized two-dimensional electron gas. *Nat. Nanotechnol.* **2018**, *13*, 915.
- (11) Fornieri, A.; Whiticar, A. M.; Setiawan, F.; Portolés, E.; Drachmann, A. C.; Keselman, A.; Gronin, S.; Thomas, C.; Wang, T.; Kallaher, R., et al. Evidence of topological superconductivity in planar Josephson junctions. *Nature* **2019**, *569*, 89.
- (12) Vischi, F.; Carrega, M.; Braggio, A.; Paolucci, F.; Bianco, F.; Roddaro, S.; Giazotto, F. Electron Cooling with Graphene-Insulator-Superconductor Tunnel Junctions for Applications in Fast Bolometry. *Phys. Rev. Appl.* **2020**, *13*, 054006.
- (13) Graziano, G. V.; Lee, J. S.; Pendharkar, M.; Palmstrøm, C. J.; Pribiag, V. S. Transport studies in a gate-tunable three-terminal Josephson junction. *Phys. Rev. B* **2020**, *101*, 054510.
- (14) Xiao, D.; Liu, G.-B.; Feng, W.; Xu, X.; Yao, W. Coupled spin and valley physics in monolayers of MoS₂ and other group-VI dichalcogenides. *Phys. Rev. Lett.* **2012**, *108*, 196802.

- (15) Bhowal, S.; Satpathy, S. Intrinsic orbital and spin Hall effects in monolayer transition metal dichalcogenides. *Phys. Rev. B* **2020**, *102*, 035409.
- (16) Žutić, I.; Fabian, J.; Sarma, S. D. Spintronics: Fundamentals and applications. *Rev. Mod. Phys.* **2004**, *76*, 323.
- (17) Wang, Q. H.; Kalantar-Zadeh, K.; Kis, A.; Coleman, J. N.; Strano, M. S. Electronics and optoelectronics of two-dimensional transition metal dichalcogenides. *Nat. Nanotechnol.* **2012**, *7*, 699.
- (18) Kormányos, A.; Zólyomi, V.; Drummond, N. D.; Burkard, G. Spin-orbit coupling, quantum dots, and qubits in monolayer transition metal dichalcogenides. *Phys. Rev. X* **2014**, *4*, 011034.
- (19) Qiu, D. Y.; Felipe, H.; Louie, S. G. Optical spectrum of MoS₂: many-body effects and diversity of exciton states. *Phys. Rev. Lett.* **2013**, *111*, 216805.
- (20) Kormányos, A.; Burkard, G.; Gmitra, M.; Fabian, J.; Zólyomi, V.; Drummond, N. D.; Fal'ko, V. k·p theory for two-dimensional transition metal dichalcogenide semiconductors. *2D Mater.* **2015**, *2*, 022001.
- (21) Tang, S.; Zhang, C.; Wong, D.; Pedramrazi, Z.; Tsai, H.-Z.; Jia, C.; Moritz, B.; Claassen, M.; Ryu, H.; Kahn, S., et al. Quantum spin Hall state in monolayer 1T'-WTe₂. *Nat. Phys.* **2017**, *13*, 683.
- (22) Miserev, D.; Klinovaja, J.; Loss, D. Exchange intervalley scattering and magnetic phase diagram of transition metal dichalcogenide monolayers. *Phys. Rev. B* **2019**, *100*, 014428.
- (23) Pisoni, R.; Kormányos, A.; Brooks, M.; Lei, Z.; Back, P.; Eich, M.; Overweg, H.; Lee, Y.; Rickhaus, P.; Watanabe, K., et al. Interactions and magnetotransport through spin-valley coupled Landau levels in monolayer MoS₂. *Phys. Rev. Lett.* **2018**, *121*, 247701.
- (24) Pisoni, R.; Lei, Z.; Back, P.; Eich, M.; Overweg, H.; Lee, Y.; Watanabe, K.; Taniguchi, T.;

- Ihn, T.; Ensslin, K. Gate-tunable quantum dot in a high quality single layer MoS₂ van der Waals heterostructure. *Appl. Phys. Lett.* **2018**, *112*, 123101.
- (25) Marega, G. M.; Zhao, Y.; Avsar, A.; Wang, Z.; Tripathi, M.; Radenovic, A.; Kis, A. Logic-in-memory based on an atomically thin semiconductor. *Nature* **2020**, *587*, 72–77.
- (26) Island, J. O.; Steele, G. A.; van der Zant, H. S.; Castellanos-Gomez, A. Thickness dependent interlayer transport in vertical MoS₂ Josephson junctions. *2D Mater.* **2016**, *3*, 031002.
- (27) Trainer, D. J.; Wang, B.; Bobba, F.; Samuelson, N.; Xi, X.; Zasadzinski, J.; Nieminen, J.; Bansil, A.; Iavarone, M. Proximity-Induced Superconductivity in Monolayer MoS₂. *ACS nano* **2020**, *14*, 2718.
- (28) Costanzo, D.; Jo, S.; Berger, H.; Morpurgo, A. F. Gate-induced superconductivity in atomically thin MoS₂ crystals. *Nat. Nanotechnol.* **2016**, *11*, 339.
- (29) Roch, J. G.; Froehlicher, G.; Leisgang, N.; Makk, P.; Watanabe, K.; Taniguchi, T.; Warburton, R. J. Spin-polarized electrons in monolayer MoS₂. *Nat. Nanotechnol.* **2019**, *14*, 432.
- (30) Cui, X.; Lee, G.-H.; Kim, Y. D.; Arefe, G.; Huang, P. Y.; Lee, C.-H.; Chenet, D. A.; Zhang, X.; Wang, L.; Ye, F., et al. Multi-terminal transport measurements of MoS₂ using a van der Waals heterostructure device platform. *Nat. Nanotechnol.* **2015**, *10*, 534.
- (31) Allain, A.; Kang, J.; Banerjee, K.; Kis, A. Electrical contacts to two-dimensional semiconductors. *Nat. Mater.* **2015**, *14*, 1195–1205.
- (32) Schauble, K.; Zakhidov, D.; Yalon, E.; Deshmukh, S.; Grady, R. W.; Cooley, K. A.; McClellan, C. J.; Vaziri, S.; Passarello, D.; Mohny, S. E.; Toney, M. F.; Sood, A.; Salleo, A.; Pop, E. Uncovering the Effects of Metal Contacts on Monolayer MoS₂. *ACS Nano* **2020**, *14*, 14798–14808.
- (33) Samm, J.; Gramich, J.; Baumgartner, A.; Weiss, M.; Schönenberger, C. Optimized fabrication and characterization of carbon nanotube spin valves. *J. Appl. Phys.* **2014**, *115*, 174309.

- (34) Lembke, D.; Bertolazzi, S.; Kis, A. Single-layer MoS₂ electronics. *Acc. Chem. Res.* **2015**, *48*, 100.
- (35) Seredinski, A.; Arnault, E.; Costa, V.; Zhao, L.; Larson, T.; Watanabe, K.; Taniguchi, T.; F.Amet,.; Newaz, A.; ; Finkelstein, G. One-Dimensional Edge Contact to Encapsulated MoS₂ with a Superconductor. *arXiv*: **2021**, 2101.06194.
- (36) Telford, E. J.; Benyamini, A.; Rhodes, D.; Wang, D.; Jung, Y.; Zangiabadi, A.; Watanabe, K.; Taniguchi, T.; Jia, S.; Barmak, K., et al. Via method for lithography free contact and preservation of 2D Mater. *Nano Lett.* **2018**, *18*, 1416.
- (37) Witcomb, M.; Dew-Hughes, D. The σ -phase in molybdenum-rhenium; microstructure and superconducting hysteresis. *J. Less-Common Met.* **1973**, *31*, 197.
- (38) Sundar, S.; Sharath Chandra, L.; Sharma, V.; Chattopadhyay, M.; Roy, S. Electrical transport and magnetic properties of superconducting Mo 52 Re 48 alloy. AIP Conference Proceedings. 2013; pp 1092–1093.
- (39) Singh, V.; Schneider, B. H.; Bosman, S. J.; Merks, E. P.; Steele, G. A. Molybdenum-rhenium alloy based high-Q superconducting microwave resonators. *Appl. Phys. Lett.* **2014**, *105*, 222601.
- (40) Pillet¹, J.-D.; Quay, C. H. L.; Morfin, P.; Bena, C.; Yeyati, A. L.; Joyez, P. Andreev bound states in supercurrent-carrying carbon nanotubes revealed. *Nat. Physics* **2010**, *6*, 965.
- (41) Gramich, J.; Baumgartner, A.; Schönenberger, C. Andreev bound states probed in three-terminal quantum dots. *Phys. Rev. B* **2017**, *96*, 195418.
- (42) Jünger, C.; Baumgartner, A.; Delagrangé, R.; Chevallier, D.; Lehmann, S.; Nilsson, M.; Dick, K. A.; Thelander, C.; Schönenberger, C. Spectroscopy of the superconducting proximity effect in nanowires using integrated quantum dots. *Commun. Phys.* **2019**, *2*, 1.

- (43) Heedt, S.; Quintero-Pérez, M.; Borsoi, F.; Fursina, A.; van Loo, N.; Mazur, G. P.; Nowak, M. P.; Ammerlaan, M.; Li, K.; Korneychuk, S., et al. Shadow-wall lithography of ballistic superconductor-semiconductor quantum devices. *arXiv preprint arXiv:2007.14383* **2020**,
- (44) Blonder, G.; Tinkham, M.; Klapwijk, T. Transition from metallic to tunneling regimes in superconducting microconstrictions: Excess current, charge imbalance, and supercurrent conversion. *Phys. Rev. B* **1982**, *25*, 4515.
- (45) Dynes, R.; Narayanamurti, V.; Garno, J. P. Direct measurement of quasiparticle-lifetime broadening in a strong-coupled superconductor. *Phys. Rev. Lett.* **1978**, *41*, 1509.
- (46) Skalski, S.; Betbeder-Matibet, O.; Weiss, P. Properties of Superconducting Alloys Containing Paramagnetic Impurities. *Phys. Rev.* **1964**, *136*, A1500.
- (47) Gramich, J.; Baumgartner, A.; Schönenberger, C. Subgap resonant quasiparticle transport in normal-superconductor quantum dot devices. *Appl. Phys. Lett.* **2016**, *108*, 172604.
- (48) Gramich, J.; Baumgartner, A.; Schönenberger, C. Resonant and inelastic Andreev tunneling observed on a carbon nanotube quantum dot. *Phys. Rev. Lett.* **2015**, *115*, 216801.
- (49) Sun, Q.-f.; Wang, J.; Lin, T.-h. Resonant Andreev reflection in a normal-metal–quantum-dot–superconductor system. *Phys. Rev. B* **1999**, *59*, 3831.
- (50) Zhitlukhina, E.; Devyatov, I.; Egorov, O.; Belogolovskii, M.; Seidel, P. Anomalous inner-gap structure in transport characteristics of superconducting junctions with degraded interfaces. *Nanoscale Res. Lett.* **2016**, *11*, 1.